Nuclear Materials and Energy 12 (2017) 1152–1156

Contents lists available at ScienceDirect

Nuclear Materials and Energy

journal homepage: www.elsevier.com/locate/nme

# Stability and propagation of the high field side high density front in the fluctuating state of detachment in ASDEX Upgrade

P. Manz[a,b,*], S. Potzel[a], F. Reimold[c], M. Wischmeier[b], ASDEX Upgrade Team[a,b,c]

[a] Physik-Department E28, Technische Universität München, James-Franck-Str. 1, 85748 Garching, Germany
[b] Max-Planck-Institut für Plasmaphysik, Boltzmannstr. 2, 85748 Garching, Germany
[c] Institute of Energy and Climate Research-Plasma Physics, Forschungszentrum Jülich GmbH, 52425 Jülich, Germany

ARTICLE INFO

*Article history:*
Available online 26 October 2016

ABSTRACT

During detachment a structure of strongly enhanced density develops close to the inner target. Its dynamics is approximated by those of radiative fluctuations appearing at a similar position and studied by means of a time-delay-estimation technique in the ASDEX Upgrade tokamak. Compared to theory the dynamics can be described as follows: at increasing density the ionization front moves upstream to reduce ionization radiation in order to balance the increased recombination radiation. The recombination zone stays close to the target strike point. The parallel motion of the ionization front is determined by the perpendicular neutral motion. The divertor nose constitutes an obstacle for the perpendicular neutral flux from the target to the region above the X-point. Passing into this shadow the neutral flux above the X-point is strongly reduced, the ionization front fades away and the heat flux from upstream can increase the temperature in the recombination region, subsequently reducing recombination and reforming an ionization front below the X-point. A cyclic reformation of the ionization front propagating from below to above the X-point occurs leading to a fluctuation as observed in the experiment.



## 1. Detachment process in ASDEX Upgrade

For magnetically confined fusion devices such as ITER the power load on the foreseen divertor target material, tungsten, must be kept below $P \approx 10$ MWm$^{-2}$, which can be only achieved under detached or partially detached conditions [1]. Recently, stable completely detached H-mode plasmas have been demonstrated in ASDEX Upgrade (AUG) [2,3]. In detached conditions modeling results show the development of a so-called virtual target regime, in which adjacent strong ionization and recombination regions are observed [4]. The strong volumetric recombination lets the virtual target act like the actual one at the wall and it is proposed to take advantage of this virtual target instead of the target plate. This investigation concerns the dynamics and stability of the virtual target, hence directly the stability of (partial) detachment, which is most crucial for the operation of magnetically confined fusion reactors.

The detachment process as observed in ASDEX Upgrade (AUG) can be divided in three states [5] as explained in the following. The given parameters relate to L-mode conditions [5], but the phenomenon is seen in both L-mode [5] and H-mode [2]. The line averaged density levels given in the following depend on the heat power and serve for rough orientation. At a line averaged density of about $\bar{n}_e \approx 1.5 \cdot 10^{19}$ m$^{-3}$, the so-called onset state (OS), the inner divertor is partially detached and the outer divertor is still attached. Then ($\bar{n}_e \approx 2.3 \cdot 10^{19}$ m$^{-3}$) in the fluctuating state (FS), strong fluctuations called X-point fluctuations in the radiated power appear. The radiation comes from a strongly localized region around and below the X-point, called the high field side high density (HFSHD) region. The frequency of these fluctuations is consistent with a wave propagating along the field lines from the X-point to the inner divertor plate with the ion sound speed [5]. As will be shown later, these structures are actually propagating in direction from the target towards the X-point and are not simple ion-acoustic waves. In addition, an increase in the electron density ($n_e \approx 2.5 \cdot 10^{20}$ m$^{-3}$) close to the X-point and an increase in the ion flux at the inner target at a distance of about 4 cm from the strike point are observed. The electron pressure at the outer divertor increases by a factor of two. Finally, in the complete detachment state (CDS) ($\bar{n}_e \approx 3.5 \cdot 10^{19}$ m$^{-3}$) the fluctuations disappear and the outer divertor detaches. The HFSHD region has moved towards the wall on the HFS above the X-point. In H-mode plasmas

* Corresponding author.
*E-mail address:* peter.manz@ipp.mpg.de (P. Manz).

http://dx.doi.org/10.1016/j.nme.2016.10.002

**Table 1**
Time lags of cross-correlation analysis of different LOSs with a reference LOS (S2L1A12) and corresponding velocity with respect to the parallel connection length to the reference position taken at the intersection of $\rho_{pol} = 1.00045$ with the reference LOS.

| LOS | Time lag ($\mu$ s) | Correlation | Velocity (km/s) |
|---|---|---|---|
| S2L3A04 | 186.8 ± 5.8 | 0.45 ± 0.05 | 20 |
| S2L3A05 | 4.7 ± 5.6 | 0.71 ± 0.07 | 400 |
| S2L3A06 | 9.2 ± 5.8 | 0.87 ± 0.04 | 820 |
| S2L1A15 | −66.7 ± 5.0 | 0.51 ± 0.07 | 60 |
| S2L1A14 | −57.1 ± 5.0 | 0.58 ± 0.07 | 50 |
| S2L1A13 | −28.9 ± 3.5 | 0.70 ± 0.05 | 70 |
| S2L1A12 | 0.0 ± 0.0 | 1.00 ± 0.00 | ref |
| S2L1A11 | 16.7 ± 4.1 | 0.79 ± 0.06 | 410 |
| S2L1A10 | 19.2 ± 7.6 | 0.71 ± 0.09 | n.a. |
| S2L1A09 | 18.8 ± 7.6 | 0.65 ± 0.08 | n.a. |
| S2L1A08 | 18.3 ± 8.2 | 0.56 ± 0.09 | n.a. |
| S2L1A07 | 16.4 ± 5.2 | 0.54 ± 0.06 | 4130 |
| S2L1A06 | 20.1 ± 5.8 | 0.48 ± 0.05 | 3490 |
| S2L1A05 | 25.0 ± 6.2 | 0.44 ± 0.03 | 2890 |
| S2L1A04 | 23.0 ± 6.4 | 0.53 ± 0.04 | 320 |

in AUG complete detachment can only be achieved with impurity seeding so far [2].

The phenomenology is the same in standard and reversed toroidal magnetic field configuration. Also it is not restricted to ASDEX Upgrade and appears also in JET [6]. Beside its relevance for ITER and DEMO, the dynamics of the HFSHD region may be critical for the proposed experiment ADX [7], where high current drive from RF launchers installed at the high field side are planed. Here, the HFSHD region due to its high cut-off frequency may hamper or even inhibit such a scenario.

In the present contribution the dynamics during the fluctuating state of detachment is studied in AUG in detail. By means of time-delay-estimation (TDE) the dynamics of the HFSHD has been studied and compared to theory [8–10]. Based on consistency with this theory and previous experiments [2,5] a model for the fluctuating state of detachment has been developed.

## 2. Experiment

### 2.1. Time delay estimation

The X-point fluctuations appear at a rather low frequency for plasma instabilities, but also at a rather high frequency for equilibrium related phenomena. To relate the fluctuations to an instability or to equilibrium effects, the dynamics of the X-point fluctuations has been analyzed in detail via fast AXUV diode bolometers [11] measuring the radiation between 1 eV and 8 keV. The sampling rate is 200 kHz. The dominant flow dynamics can be inferred by a time delay estimation technique via cross-correlation of different lines of sights (LOSs) with a reference LOS (S2L1A12) located close to the X-point. This reference LOS has been chosen for two reasons, first the X-point fluctuations are most prominent for this LOS [5] and this LOS measures at the high-field-side (HFS) and allows to discriminate low-field-side (LFS) and HFS dynamics. The positions of the analysed LOSs of the fast AXUV diode bolometers in the poloidal cross-section of AUG are shown in Fig. 1. The time lags reflect the temporal sequence in which the structure is located at a given LOS with respect to the fixed reference LOS. The structure moves from left to right corresponding to a movement from high field side to low field side as can be seen at the sequence S2L1A15 → S2L1A14 → S2L1A13 → S2L1A12 (Table 1). The movement could be even go through the X-point or private flux region. The structure moves from bottom to top (S2L3A05 → S2L1A12 → S2L5A06 (Table 1)). A structure bound to a magnetic field line in the HFS SOL moves upstream from the target to the X-point and

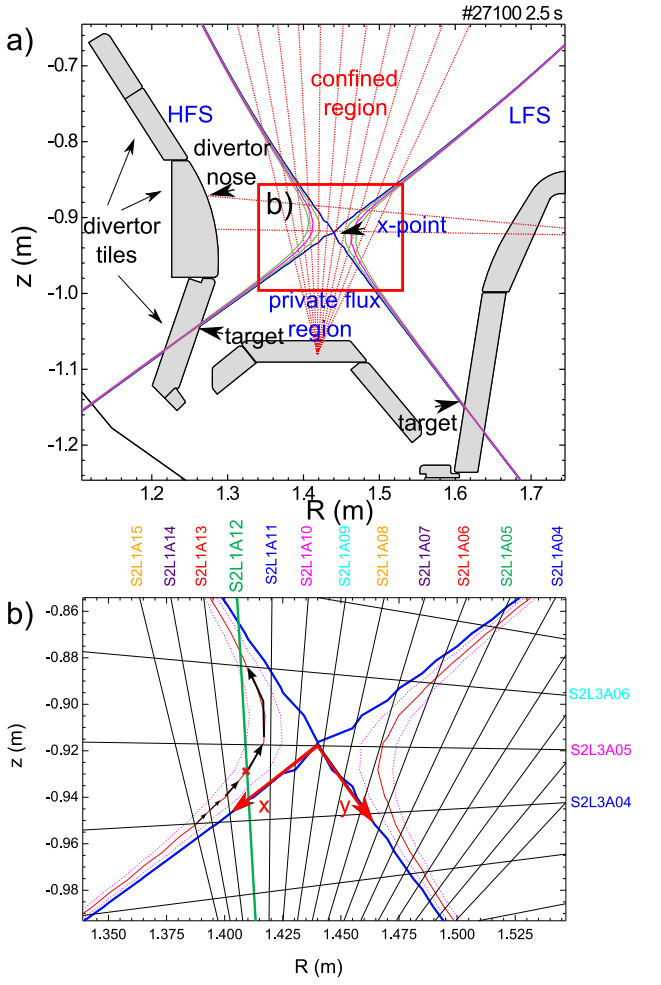


**Fig. 1.** a) Divertor geometry of ASDEX Upgrade. b) Section near the X-point of the poloidal cross-section of AUG including the analysed LOSs of the fast AXUV diode bolometers. The red solid line shows a reference flux surface at $\rho_{pol} = 1.0010$, the magenta dotted lines show neighboring flux surfaces. The black arrows illustrate the basic movement of a structure bound to a magnetic field line. The X-point coordinate system ($x$, $y$) is shown by the red arrows at the X-point as its origin. (For interpretation of the references to color in this figure legend, the reader is referred to the web version of this article.)

further upstream as indicated by the arrows in Fig. 1. Choosing a different LOS (for example S2L3A05) does not change the observed dynamics.

If the distance between the different positions is known the time lag can be interpreted as a velocity. A propagation path has to be assumed and the result can be evaluated based on consistency. In the following subsection a parallel propagation first and in the subsequent subsection a perpendicular propagation is assumed.

### 2.2. Assumed parallel propagation

For ion sound or Alfvén waves a purely parallel propagation would be a reasonable assumption and the distance of the LOSs can be estimated by the parallel connections length of the field lines. The corresponding parallel velocities for a flux surface at $\rho_{pol} = 1.00045$ are shown in Table 1. The results do depend on the chosen flux surface. By varying the reference position and taking into account the uncertainties in the time lag the velocities can be estimated within a factor of two to three. Below the X-point the structures propagate with 50–70 km/s (S2L1A15-S2L1A13), which is slightly above the estimated ion sound speed of $c_{si} = \sqrt{(T_e + T_i)/m_i} = 38$ km/s assigning electron and ion temper-

atures $T_e = T_i$ of 15 eV [5]. This corresponds within uncertainties to the ion sound speed. Approaching the X-point the structures strongly accelerate reaching parallel signal velocities up to 800 km/s above the X-point. Obviously these structures are not ion-acoustic waves.

The high velocities may point to Alfvénic waves. The corresponding density for the Alfvén velocity is $n_e \approx 2.5 \cdot 10^{21}$ m$^{-3}$, i.e. one order of magnitude larger as observed in the present discharge. However, it should be noted that even these high densities have been observed in the HFS scape-off layer in AUG, but at higher heating powers. Indeed, around the divertor poloidal magnetic field fluctuations $\dot{B}_\theta$ are observed. But those appear at around 30–50 kHz, and no fluctuations around the X-point fluctuation frequency in the low kHz range are detected. A further cross-coherence analysis not shown here reveals that high coherence between different LOSs is exclusively found at the X-point fluctuation frequency and the coherence around 30–50 kHz is rather low. Therefore the structure observed with the time-delay estimation technique depicts the dynamics of the HFSHD, which is neither connected to ion-acoustic nor to Alfvénic waves.

### 2.3. Assumed perpendicular propagation

It is important to note that in a tokamak parallel to the magnetic field line is not toroidal and perpendicular is not poloidal. Close to the X-point the toroidal direction is nearly parallel, but the perpendicular direction on a magnetic flux surface is not poloidal as seen in Fig. 1b. Also an approximation of the parallel direction by the toroidal direction is problematic as the strong parallel gradients in density and temperature as described in the next section cannot be in the toroidal direction as a tokamak is still toroidally symmetric. Standard flux coordinates are singular around the X-point. Because of these reasons the dynamics of the HFSHD region is investigated in the X-point coordinate system developed by Mattor [9] similar to those used by Ryutov and Cohen [12]. This is inferred from supplementary radial, poloidal and toroidal $(\psi, \chi, \varphi)$ flux coordinates which are orthogonal but not straight field line coordinates. The X-point coordinates $(x, y)$ used here are described in Ref. [9]. They are given by a family of hyperbolas, where the poloidal flux is given by $\psi = xy$ and the perpendicular coordinate by $\chi = (y^2 - x^2)/2$, with metric factors defined by $\nabla\psi = \mathbf{e}_\psi / h_\psi$, $\nabla\chi = \mathbf{e}_\chi / h_\chi$ and $\mathbf{e}_\chi = \mathbf{e}_\psi \times \mathbf{e}_\varphi$. The metric factor may be approximated by $h_\psi = h_\chi = B_\theta / l_d$, poloidal magnetic field $B_\theta$ taken at the top of the machine [13] and distance from X-point to the divertor plate $l_d$ [12] or $B_\theta / l_d$ may be approximated by the local gradient at the X-point $\nabla B_\theta$. As seen in Fig. 1b, the HFS X-point region is characterized by $x > 0$ and $y < 0$, where both tend to lower values at the X-point $(x \to 0, y \to 0)$, upstream positions towards the HFS midplane are characterized by $x \to 0$, $y \ll 0$ and the inner target by $x \gg 0$, $y \to 0$.

For the specific L-mode discharge [5] for which we did the time delay analysis here, the $x$-axis is estimated as $z = 0.718 \cdot R - 1.958$ m, the $y$-axis as $z = -1.470 \cdot R + 1.205$ m with the X-point at $(R_X, z_X) = (1.446, -0.920)$ m (intersection of x- and y-axis). The distance to the $x$-axis gives the $y$ value and the distance to the $y$-axis gives the $x$ value of the X-point coordinates. All points are close to a hyperbola with $xy \approx 345$ mm$^2$. This distance between the reference point along this hyperbola (constant $xy = 345$ mm$^2$) can be estimated by $L_X = \int_{y(ref)}^{y} \sqrt{1 + (\frac{xy}{y^2})^2}\, dy$. Corresponding perpendicular velocities in X-point geometry can be estimated by dividing the distance by the previously estimated time lag. Results are listed in Table 2. Below the X-point low perpendicular velocities of 400 to 500 m/s are observed. Assuming a neutral temperature of 5 eV the neutral sound speed is about 15 km/s. The perpendicular motion would be one tenth of the order of magnitude of the sound speed. Upstream the X-point the velocities increases up to ≈ 5.5 km/s which is of the order of the neutral sound speed.

**Table 2**
Time lags of a cross-correlation analysis of different LOSs with a reference LOS (S2L1A12), positions in the $(R, z)$-plane, X-point coordinates $(x, y)$, distances $L_x$ to the reference position along a hyperpola $xy = 345$. The reference position and positions in the $(R, z)$-plane, X-point coordinates $(x, y)$, respectively are taken at the intersection of $\rho_{pol} = 1.00045$ with the reference LOS.

| LOS | R (m) | z (m) | y (mm) | x (mm) | $L_X$ (mm) | $v_{\perp,X}$ (km/s) |
|---|---|---|---|---|---|---|
| S2L1A15 | 1.388 | −0.956 | 5 | 67 | 35 | 0.52 |
| S2L1A14 | 1.394 | −0.949 | 6 | 59 | 23 | 0.40 |
| S2L1A13 | 1.402 | −0.943 | 7 | 49 | 15 | 0.51 |
| S2L1A12 | 1.410 | −0.934 | 10 | 37 | 0 | – |
| S2L3A05 | 1.420 | −0.918 | 17 | 20 | 16 | 3.40 |
| S2L3A06 | 1.413 | −0.884 | 48 | 7 | 50 | 5.44 |

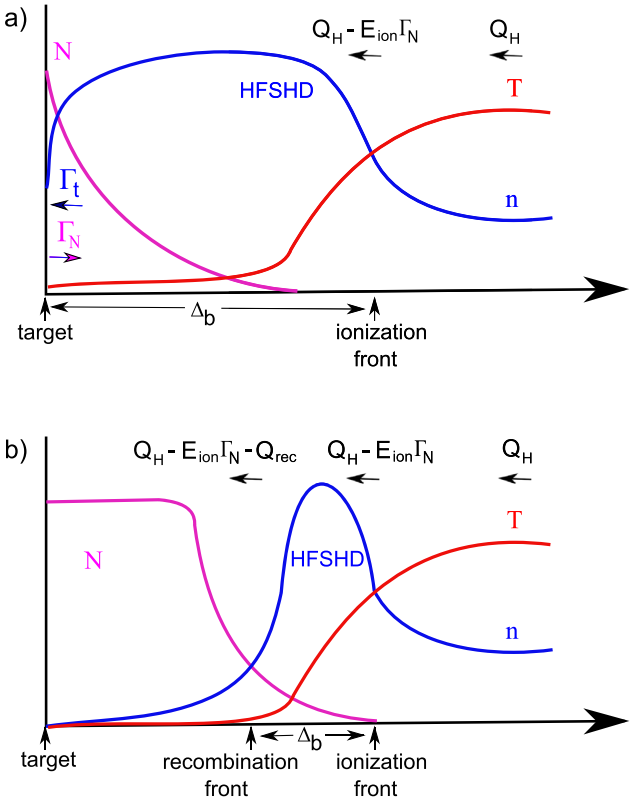


**Fig. 2.** High field side density front (HFSHD) in the case, (a) where the plasma neutralized at the target and (b) the plasma recombines volumetrically (adapted from Ref. [8]).

## 3. Comparison with theory

Changes in the quasi-equilibrium can lead to a movement of the ionization-recombination front. Ionization and recombination fronts are defined here as the position along the magnetic field line where ionization and recombination rates strongly increase, respectively. Therefore the above described results are compared with the theory by Krasheninnikov [8] slightly modified to better fit the AUG conditions. As depicted in Fig. 2a, in the high recycling regime the power $Q_H$ is conducted into the ionization front. Each ionization of a neutral particle results in an energy loss of $E_{ion}$ and the ionization front reduces the power flux with a rate of $E_{ion}\Gamma_N$, where $\Gamma_N$ is the neutral flux into the ionization front. In fact, in the high recycling regime in stationary state the neu-

tral recycled flux from the target is equal to the ion flux to the target $\Gamma_t$. With increasing plasma density the ion flux to the target increases and therefore also the neutral flux into the ionization front. This in turn reduces the thermal power flux towards the target to $Q_t = Q_H - E_{ion}\Gamma_t$. We see $Q_H > E_{ion}\Gamma_t$. Between the target and the ionization front a dense cold plasma buffer (the region of enhanced plasma density corresponds to the HFSHD) exists. Due to the high density and low temperature recombination cannot be neglected resulting in an additional energy loss $Q_{rec}$ as depicted in Fig. 2b. Therefore, the power at the ionization front has to fulfill $Q_H > E_{ion}\Gamma_N + Q_{rec}$ or $Q_H - Q_{rec} > E_{ion}\Gamma_N$. With increasing density $Q_{rec}$ increases. To fulfill the balance $Q_H - Q_{rec} > E_{ion}\Gamma_N$ the neutral flux $\Gamma_N$ has to reduce. Actually, recombination is not necessary for this argumentation. Instead of the ionization energy the radiative energy loss per ionization is important. In collisional-radiative models multi-step ionization from excited states is considered. The population density of the excited states depends on the plasma density. For increasing plasma density the radiative energy losses per ionization increase, which leads to the necessary reduction in the neutral flux $\Gamma_N$. However, for simplicity we assume $E_{ion}$ constant. As $\Gamma_N \sim \sqrt{T_b}/\Delta_b$ as derived in Ref. [8] either the temperature $T_b$ (assumed the same for all species) in the high field side density front must reduce, which facilitates recombination and would result in even lower temperatures or the distance between the neutral particle source (mainly the target) and the ionization front $\Delta_b$ has to increase (Fig. 2). Below a certain temperature threshold recombination becomes a heating term for the electrons due to three body recombination. Also in this case the temperature is limited and cannot drop and an increase of $\Delta_b$ is necessary. Such an increase in $\Delta_b$ corresponds to a displacement of the ionization front towards the X-point. Dynamically this constitutes a propagation. Two timescales determine this propagation: first the parallel heat conduction, which is carried by the high-energetic electrons [14,15] and the neutral flux from downstream entering the ionization front. Obviously, the neutral flux is the slower timescale and will determine the dynamics. The reaction of the neutrals can be expected to be bound by their sound speed $c_N = \sqrt{T_N/m_i}$. As the neutral motion is not bound to the field lines, they do not have to follow the long parallel distances, but they cut short perpendicular to the magnetic field. The propagation velocity of the ionization front has been predicted to be of order of the neutral sound speed [8]. It stops at the position $Q_H - E_{ion}\Gamma_N = Q_{rec} + Q_t$, where the energy balance is fulfilled. In the case of ideal detachment $Q_t \ll Q_{rec}$ the position dependents mainly on $Q_{rec} \sim n_e^2$ and the position moves upstream with increasing density. The observed low perpendicular velocities of 400 to 500 m/s below the X-point are much below the predicted value of dynamic processes in the order of the ion or neutral sound speeds, which points to a working point close to the equilibrium. Upstream the X-point the velocities of up to $\approx$ 5.5 km/s are in the order of the neutral sound speed. This points to a dynamical reformation of the front structure.

With increasing density the temperature drop starts earlier and the distance $\Delta_b$ increases. At some point the ionization front appears above the X-point. The divertor nose provides an obstacle for the neutral particles from the target strike line or the recombination region. By propagating upstream the ionization front will propagate at some point into a shadow of the recycled neutral flux. As otherwise $\Delta_b$ cannot be increased the recombination front is not allowed to move with the ionization front. The main neutral source is either the strike line or the recombination region which has to stay close to the strike point anyhow. The movement into a neutral shadow ($\Gamma_N \rightarrow 0$) will lead to a collapse of the ionization loss $E_{ion}\Gamma_N$. This is unproblematic for the energy balance as $Q_H - Q_{rec} \gg 0$. Subsequently, the heat flux $Q_H$ will hit the plasma density enhancement leading to an increase in temperature and reduction of recombination losses $Q_{rec}$. A new equilibrium has to be established at reduced $Q_{rec}$ and increased $E_{ion}\Gamma_N$, which can be only found downstream. At strongly reduced $\Delta_b$ an equilibrium with reduced radiation losses is possible. Hence the ionization front is again closer to the recombination front. The ionization front will reestablish downstream. The neutral motion does not set the limit for the back movement as enough neutrals can be expected to be present downstream and the dynamics is set by the electron heat conduction. Due to the fast time scale of the heat conduction the ionization front jumps back to its original position. This occurs too fast to be resolved with the AXUV diode bolometer system and explains why only the movement in the upstream direction is seen in the TDE correlation pattern.

A stable detachment is therefore only possible if the recombination front moves to the X-point or above preventing such a shadow. The appearance of recombination at the X-point is also observed for complete detachment [5] coinciding with stable detached conditions at the inner divertor. As the recombination front cannot overtake the ionization front an additional neutral source above the strike point in the far SOL is necessary for neutral supply above the X-point. Then, the ionization front can move upstream from the X-point towards the inner midplane allowing the recombination front to proceed to the X-point.

Next, possibilities for a neutral supply above the X-point in the far SOL will be discussed, where the actual neutral supply will be a combined effect. First, the recycled particle flux from the strike line can diffuse behind the divertor and leakage between the divertor tiles into the chamber leading to localized upstream neutral sources (see geometry as depicted in Fig. 1a). Neutral leakage should be present during the whole process and not be restricted to the movement of the ionization front above the X-point. Second, filamentary transport at the low field side can lead to higher electron temperatures in the far SOL upstream. Thus, higher $Q_H$ and higher densities can be expected resulting in a higher recycled particle flux from the position where the filaments are connected to the divertor nose at the HFS. Indeed, before complete detachment the filaments are getting very large and fast at the low field side [16] leading to a reasonable perpendicular particle flux (about 25% to 45% of the total recycled particle flux [17]) as well as to a even stronger contribution to the perpendicular power flux (about equal to even above its contribution to the divertor target [17]).

## 4. Summary

Based on a time delay estimation of different lines of sight of fast AXUV diode bolometers in comparison with previous studies [2,5] and theory [8–10] the HFS detachment process in AUG can be imagined as illustrated in Fig. 3 and described in the following:

In the onset state (Fig. 3a), to compensate energy losses due to enhanced recombination radiation at increasing density the distance between ionization and recombination front $\Delta_b$ has to increase [8]. Therefore only the ionization front (the HFSHD) propagates upstream. The timescale is preset by the neutral influx $\Gamma_N$ into the ionization front from downstream, where the neutral dynamics is not bound to the field line geometry and therefore small perpendicular velocities are sufficient to explain the observed velocities from the time-delay estimation technique.

If the HFSHD region propagates upstream of the X-point the neutral flux is shaded due to the divertor geometry (Fig. 3b). At low neutral influx the ionization front fades away. However, without ionization losses the heat flux from upstream $Q_H$ directly penetrates into the recombination volume leading to an increase in temperature, decrease in density and recombination radiation. This gives rise to an equilibrium with strongly reduced $\Delta_b$. The ionization front redevelops downstream of the X-point. Cyclic extinction of the ionization front above the X-point together with its reformation below the X-point and the subsequent propagation upstream

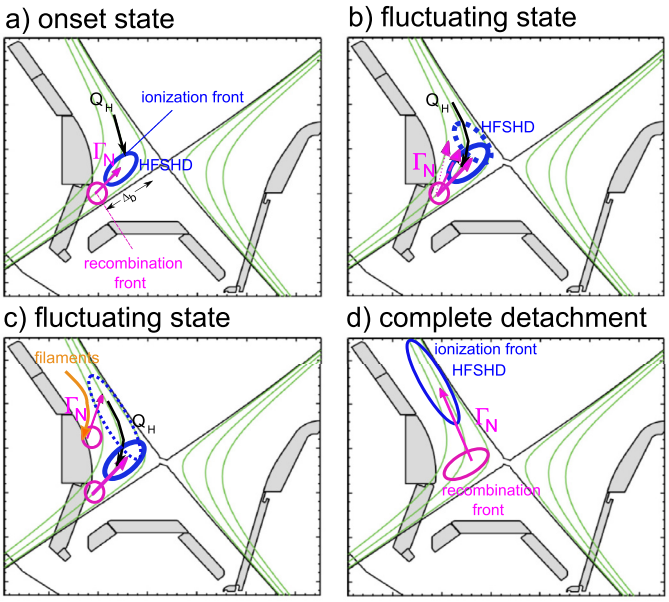


**Fig. 3.** Summary of the model of the HFS detachment process in AUG as described in the text.

results in fluctuations of the radiation similar to those observed. The cyclic propagation from below to above the X-point should occur with a maximum speed of the neutral sound speed. The observed velocities deduced via a time-delay estimation technique in X-point coordinates occur in the order of the neutral sound speed within the experimental uncertainties.

At complete detachment the recombination region is located around the X-point (Fig. 3d). At the transition form the fluctuating state to complete detached state the recombination region has to move upstream. As the recombination region cannot overtake the ionization region, the ionization region has to propagate further upstream, which is only possible with an additional neutral supply around the X-point, hence the divertor nose. Possible neutral sources can be provided by leakage between the divertor tiles and directly recycled flux due to strongly enhanced LFS filamentary transport at the far SOL [16,18]. For complete detachment the outer divertor is detached and filaments are in the inertial regime resulting in enhanced LFS filamentary transport. The plasma flux towards the wall (divertor nose) will be recycled and the neutral flux transmitted from the divertor nose can facilitate the development of an ionization front above the X-point (Fig. 3c). If the recycled neutral flux from the divertor nose is strong enough to sustain the ionization front upstream the X-point, the recombination front can succeed the ionization front and the divertor becomes transparent for neutrals. Once the recombination front is at the X-point, the neutral flux transmitted from it can sustain the ionization front itself constituting stable detached conditions at the inner divertor (Fig. 3d).

## Acknowledgements

This work has been carried out within the framework of the EUROfusion Consortium and has received funding from the Euratom research and training programme 2014–2018 under grant agreement No. 633053. The views and opinions expressed herein do not necessarily reflect those of the European Commission.

## References

[1] R.A. Pitts, et al., J. Nucl. Mat. 438 (2013) 48.
[2] F. Reimold, et al., Nucl. Fusion 55 (2015) 033004.
[3] A. Kallenbach, et al., Nucl. Fusion 55 (2015) 053026.
[4] A. Kukushkin, et al., J. Nucl. Mat. 241–243 (1997) 268.
[5] S. Potzel, et al., Nucl. Fusion 54 (2014) 013001.
[6] S. Potzel, et al., J. Nucl. Mat. 463 (2015) 541.
[7] B. LaBombard, et al., Nuclear Fusion 55 (2015) 053020.
[8] S.I. Krasheninnikov, et al., J. Nucl. Mater. 266–269 (1999) 251.
[9] N. Mattor, Phys. Plasmas 2 (1995) 594.
[10] S. Krasheninnikov, A. Smolyakov, Phys. Plasmas 15 (2008) 055909.
[11] M. Bernert, et al., Rev. Sci. Inst. 85 (2014) 033503.
[12] D.D. Ryutov, R. Cohen, Contrib. Plasma Phys. 48 (2008) 48.
[13] D. Farina, R. Pozzoli, D.D. Ryutov, Nucl. Fusion 9 (1993) 1315.
[14] P.C. Stangeby, A.W. Leonard, Nucl. Fusion 51 (2011) 063001.
[15] A.V. Chankin, D.P. Coster, G. Meisl, Contrib. Plasma Phys. 52 (2012) 500.
[16] D. Carralero, et al., Nucl. Fusion 54 (2014) 123005.
[17] T. Lunt, et al., J. Nucl. Mat. 463 (2015) 744.
[18] D. Carralero, et al., Phys. Rev. Lett. 115 (2015) 215002.